Applications in Engineering Science 5 (2021) 100036

Contents lists available at ScienceDirect

Applications in Engineering Science

journal homepage: www.elsevier.com/locate/apples

Stability domain and design of a plane metamaterial made up of a periodic mesh of rods with cross-bracing cables

Francesco Trentadue [a,*], Domenico De Tommasi [a], Nicola Marasciuolo [b]

[a] Dip. Scienze Ingegneria Civile e Architettura, Politecnico di Bari, Via Re David 200, Bari, Italy
[b] Politecnico di Bari, Via Re David 200, Bari, Italy

ARTICLE INFO

Keywords:
Metamaterials
Elastic stability
Periodic materials

ABSTRACT

In this work we examine a plane metamaterial subjected to a generic biaxial macrostress, obtained by coupling a periodic mesh of rods with a periodic mesh of extremely flexible cables. In particular, we couple a square mesh of rods with diagonal cables with the aim of enhancing the stability performance of the obtained metamaterial. By introducing appropriate restrictions on the feasible critical modes, the study can be framed into the context of the Eulerian stability analysis and then, by means of Floquet-Bloch theory, a closed form solution for the stability domain is determined. Finally, on the basis of the previous stability analysis the optimal design problem is addressed.

1. Introduction

Design of metamaterials is a very active research field for its both theoretical and technological interest. Metamaterials generally present periodic patterns at the microscale that can be designed to achieve extreme electromagnetic (Chen et al., 2010) or mechanical responses not exhibited by natural materials. Among the various extreme mechanical properties attained by metamaterials we recall vanishing macroscopic shear stiffness (Schittny et al., 2013), negative effective dynamic modulus (Fang et al., 2006), selective buckling depending on self stress (Paulose et al., 2015) and controlled propagation of mechanical waves (Bordiga et al., 2020; Cummer et al., 2016; Krushynska et al., 2017). Tunable mechanical behaviors can be also obtained by adopting microstructures based on tensegrity schemes (Amendola et al., 2018; DeTommasi et al., 2017; 2018; Fraternali et al., 2014; 2012).

In design of metamaterials a crucial point is the onset of critical equilibrium states in which periodic metamaterials exhibit critical modes with wavelengths independent from the size of cell (Geymonat et al., 1993). A rigorous approach to these instability phenomena is based on Floquet-Bloch theory and within this context several periodic systems has been studied. Among these, we recall periodical trusses and honeycombs materials, which were analyzed in Hutchinson and Fleck (2006) and Triantafyllidis and Schraad (1998), Kelvin cell foams (Gong et al., 2005) and sequential bifurcations in bilayered structures (Liu and Bertoldi, 2015). Grids of rods have been extensively studied in (Wang and McDowell, 2004) and a numerical optimization procedure for 2D periodic structures has been presented in (Boukadia et al., 2020).

The main idea of the present paper is to couple periodic patterns of rods with periodic patterns of extremely flexible cables to enhance the stability performance of the obtained metamaterial. Here a particular pattern made of a square mesh of rods has been examined, both because its mechanical performance can be significantly improved by adding diagonal cables and because a closed form solution for its stability domain can be easily searched. However, in our opinion, many periodic patterns of rods can get significantly enhanced structural performances in this way, since generally the coupling with periodic pattern of cables reduce the wave (effective) length of critical modes in rods. Furthermore, periodic microstructures of extremely flexible diagonal elements can be easy coupled with much more rigid rod elements thanks to 3D printing.

The aim of the present work is then to determine the stability domain of the above described metamaterial (see Fig. 1) and subsequently address its design. In the simpler case of absence of cables, closed form solutions for the stability domain were obtained in (Haghpanah et al., 2014), where the wave length of the critical modes was assigned *a priori* in order to avoid a complete Floquet-Bloch analysis. Here, by means of some simplifying assumptions, suitable restrictions on the feasible critical modes are determined, which allow us to adopt the Floquet-Bloch theory and to frame the present study into the context of the Eulerian stability analysis. With this regard, we remark that our approach can be applied only if the precritical response is almost linear, so that if critical state analysis can be carried out by simply solving an eigenvalue problem. Closed form solutions for the stability domain are given and the effectiveness of the obtained result is validated by FEM analysis.

* Corresponding author.
E-mail address: francesco.trentadue@poliba.it (F. Trentadue).

https://doi.org/10.1016/j.apples.2021.100036
Received 4 November 2020; Received in revised form 13 January 2021; Accepted 17 January 2021
Available online 20 January 2021

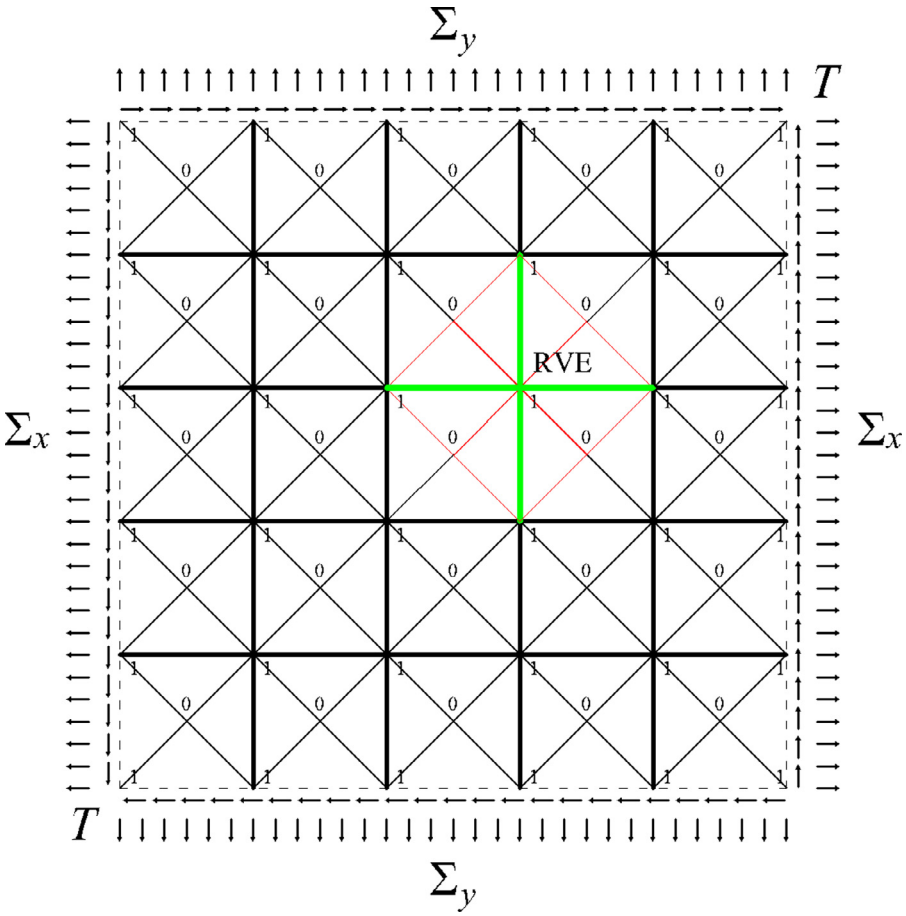

Fig. 1. Periodic material subjected to a generic macrostress and periodic cell (RVE).

Finally, the minimum thickness of the cables is determined for particular macrostress states.

2. Mechanical model

The plane periodic material shown in Fig. 1, made up of a square mesh of rods with diagonal cables, is here analyzed. The material is subjected to a generic plane macrostress.

As usual in the stability analysis of slender rods, the axial and shear deformations are neglected. Further, the bending and axial stiffnesses of cables are assumed negligible with respect to those of rods, so that the following conditions hold

$$\frac{J_c}{J} \to 0\,, \quad \frac{A_c}{A} \to 0, \tag{1}$$

where J_c and A_c are the moment of inertia and the cross section areas of the diagonal cables and J and A are those of the rods. As a consequence of (1), diagonal cables immediately buckle under compression forces.

Although this is not the only possible choice, we consider rectangular cross sections for both cables and rods. Sections have thicknesses t and t_c and unitary dimension in the direction orthogonal to the plane. Then we have

$$J = \frac{t^3}{12}, \qquad J_c = \frac{t_c^3}{12}, \qquad A = t, \qquad A_c = t_c\,. \tag{2}$$

In this periodic material (Fig. 1) we distinguish joints of type 1, connecting four rods and four cables and joints of type 0, connecting only cables. In view of the assumptions (1) in the following analysis the equilibrium of joints 0 will be neglected.

The chosen periodic cell (RVE) is shown in Fig. 1. It includes four rods of length l, four inner diagonal cables of length $l/\sqrt{2}$ and four boundary cables of length $\sqrt{2}l$, which are shared with the neighboring cells. For this reason in the following analysis their stiffnesses will be halved.

3. Equilibrium of the fundamental state

As already stated, this periodic material is subjected to a generic plane macrostress in its fundamental state. At first, let us consider the simple case in which the shear macrostress T is null. In view of (1) the traction forces in cables due to eventual macro traction states are negligible and the axial (compressive) forces in the horizontal and vertical rods are given by

$$P_{\Sigma_x} = -\Sigma_x l, \quad P_{\Sigma_y} = -\Sigma_y l\,, \tag{3}$$

where Σ_x and Σ_y are the horizontal and vertical normal traction macrostresses.

Next, let us consider a pure shear state, in which the internal forces represented in Fig. 2 occur. We recall that, as a consequence of (1), the compressed cables (thin dotted lines) immediately buckle and their axial forces vanish, whereas in the tense (active) cables, represented by thin continuous lines, the traction forces N_T are exerted. At the same time, the axial compression forces P_T and the shear forces S_T occur in both horizontal and vertical rods. In particular we find

$$N_T = \sqrt{2}\rho|T|l, \quad P_T = \rho|T|l, \quad S_T = (1-\rho)Tl, \tag{4}$$

where

$$\rho = \frac{k_e}{k_e + 12}\,. \tag{5}$$

The distribution factor ρ is determined in Appendix C and k_e is the dimensionless elastic stiffness of cables, given in Appendix B.

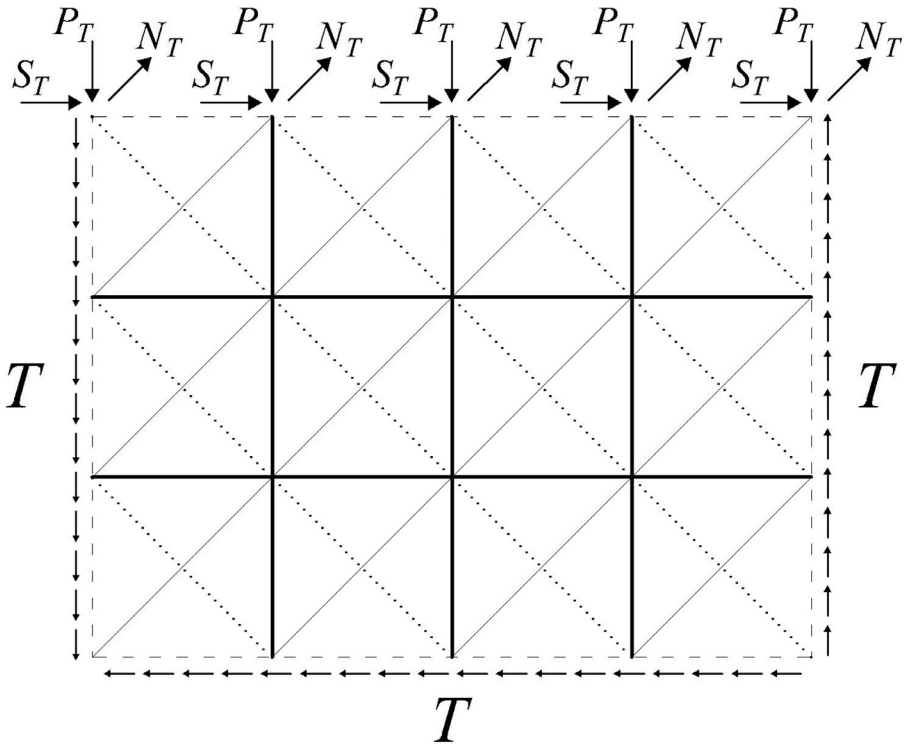

Fig. 2. Internal forces in a pure shear macrostress.

Finally, the total compression forces P_x and P_y in the horizontal and vertical rods are determined by superposition of the two cases above considered

$$P_x = P_{\Sigma_x} + P_T\,, \qquad P_y = P_{\Sigma_y} + P_T\,. \tag{6}$$

4. Bloch wave analysis

The periodic critical modes of this two dimensional lattice are now explored. The generalized joint displacement field is represented in the complex form

$$\boldsymbol{u}(\boldsymbol{x}) = \{u(\boldsymbol{x}), v(\boldsymbol{x}), \theta(\boldsymbol{x})\}^T \in \mathbb{C}^3,$$

where $\boldsymbol{x}$ is the lattice position vector

$$\boldsymbol{x} = \zeta_1 l\boldsymbol{i} + \zeta_2 l\boldsymbol{j}\,, \quad (\zeta_1, \zeta_2) \in \mathbb{Z}^2$$

and $\boldsymbol{u}(\boldsymbol{x})$ is specified over the entire lattice by means of the Bloch's theorem

$$\boldsymbol{u}(\boldsymbol{x}) = \boldsymbol{u}(\boldsymbol{0})e^{i\boldsymbol{w}\cdot(\zeta_1 l\boldsymbol{i}+\zeta_2 l\boldsymbol{j})} = \boldsymbol{u}(\boldsymbol{0})e^{i(\omega_1\zeta_1+\omega_2\zeta_2)}\,. \tag{7}$$

Here $\boldsymbol{w}$ is the wave vector and $\boldsymbol{\omega} = l\boldsymbol{w}$ is a dimensionless wave vector chosen in such a way that $\omega_1, \omega_2 \in (-\pi, \pi)$ in the first Brillouin zone.

4.1. Inextensibility constraint

Let us now consider the square mesh made by four rods and two couples cables in Fig. 3. Notice that, due to the inextensibility of rods, in the two diagonal directions the cable are alternatively tense (thin continuous lines) and buckled (thin dotted lines).

Since the vertical rods are axially inextensible, the horizontal rods develop equal *rigid* rotations, so that

$$\frac{v(\boldsymbol{x}+l\boldsymbol{i}) - v(\boldsymbol{x})}{l} = \frac{v(\boldsymbol{x}+l\boldsymbol{i}+l\boldsymbol{j}) - v(\boldsymbol{x}+l\boldsymbol{i})}{l}\,. \tag{8}$$

Then, in view of (7), we get

$$\beta_h(\boldsymbol{x})(e^{i\omega_2} - 1) = 0\,, \tag{9}$$

where

$$\beta_h(\boldsymbol{x}) = \frac{v(\boldsymbol{x}+l\boldsymbol{i}) - v(\boldsymbol{x})}{l} = \frac{e^{i\omega_1}-1}{l}v(\boldsymbol{x})\,. \tag{10}$$

In the same way we find

$$\beta_v(\boldsymbol{x})(e^{i\omega_1} - 1) = 0\,, \tag{11}$$

where

$$\beta_v(\boldsymbol{x}) = \frac{u(\boldsymbol{x}+l\boldsymbol{j}) - u(\boldsymbol{x})}{l} = \frac{e^{i\omega_2}-1}{l}u(\boldsymbol{x})\,. \tag{12}$$

The two Eqs. (9) and (11) can be simultaneously satisfied only in the following four cases:

- **i)** $u(\boldsymbol{x}) = v(\boldsymbol{x}) = 0$: the nodal translations are null and all wave parameters $\omega_1, \omega_2 \in (-\pi, \pi)$ are feasible;
- **ii)** $\beta_h = 0$ and $\omega_1 = 0$: the horizontal rods do not rotate and the wave length in horizontal direction is infinite;
- **iii)** $\beta_v = 0$ and $\omega_2 = 0$: the vertical rods do not rotate and the wave length in vertical direction is infinite;
- **iiii)** $\omega_1 = \omega_2 = 0$: the wave length is infinite in both directions. Since translational displacements are inessential in this problem, this case can be included in the more general case **i)**.

4.2. Stability analysis

Since the stiffness of a periodic cell does not depend on rigid translations, without loss of generality, the following degrees of freedom vector can be adopted

$$\boldsymbol{\gamma} = \{\beta_h, \beta_v, \theta\}^T = \{\beta_h(\boldsymbol{x}), \beta_v(\boldsymbol{x}), \theta(\boldsymbol{x})\}^T\,.$$

The hermitian stiffness matrix $\boldsymbol{k}$ of the cell is then determined as sum of a rods stiffness matrix $\boldsymbol{k}_b$ (Appendix A) and a cables stiffness matrix $\boldsymbol{k}_c$ (Appendix B). We find

$$\boldsymbol{k} = \boldsymbol{k}(\boldsymbol{\omega}, q_x, q_y)\,, \tag{13}$$

so that $\boldsymbol{k}$ depends on both the wave vector and the applied macrostress, through the parameters (see Appendix A):

$$q_x = \frac{l}{2}\sqrt{\frac{P_x}{EJ}}\,, \qquad q_y = \frac{l}{2}\sqrt{\frac{P_y}{EJ}}\,. \tag{14}$$

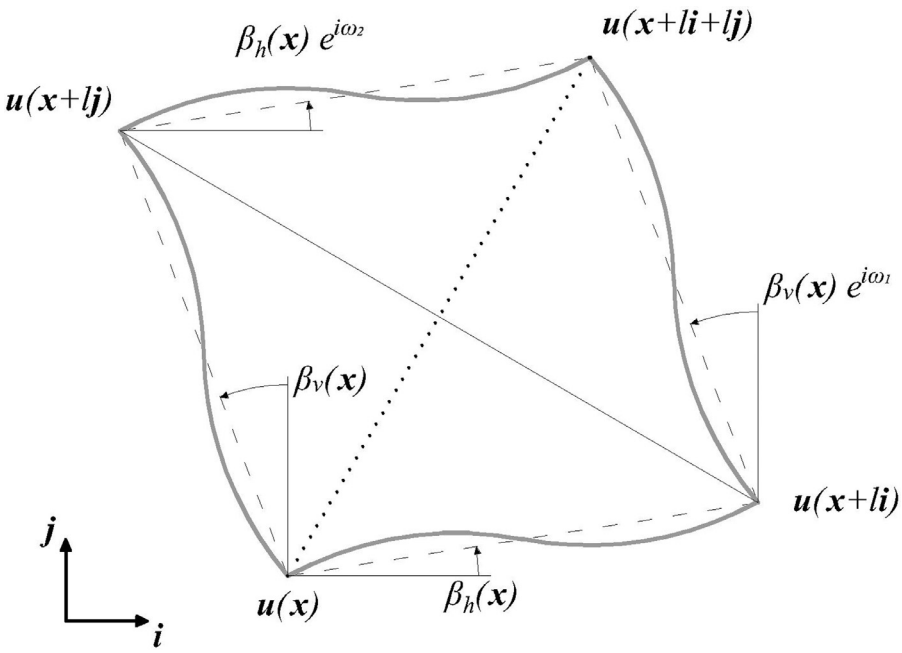

Fig. 3. A square mesh formed by four rods and two cables.

Let us denote by $(.)^*$ the conjugate of a complex quantity. We require that in all feasible (stable or critical) states the second variation of the total energy is semidefinite positive, so that for a generic cell we can write

$$\frac{1}{2}\boldsymbol{\gamma}^* \boldsymbol{k}(\boldsymbol{\omega}, q_x, q_y)\boldsymbol{\gamma} \geq 0 \tag{15}$$

and in a critical state it must be

$$\boldsymbol{k}(\boldsymbol{\omega}, q_x, q_y)\boldsymbol{\gamma} = \mathbf{0}, \quad |\boldsymbol{\gamma}| > 0. \tag{16}$$

In the following we will discuss (15) by considering separately each of the three cases **i) - iii)**.

i) From (10) and (12) we find $\beta_h = \beta_v = 0$. The stability condition (15) reduces to

$$\theta^* k_{b33}\theta = 4\theta^*\left(\frac{\Psi_x - \Phi_x \cos\omega_1}{\Psi_x^2 - \Phi_x^2} + \frac{\Psi_y - \Phi_y \cos\omega_2}{\Psi_y^2 - \Phi_y^2}\right)\theta \geq 0\,, \tag{17}$$

where the dimensionless stiffness k_{b33} and the functions Φ and Ψ are given in Appendix A. Since $\Phi(q) < 0$ and $\Phi(q)^2 - \Psi(q)^2 \geq 0$ the minimum value of k_{b33} is always attained when the two wave parameters ω_1 and ω_2 are both equal to π. Therefore from (17) we get

$$\frac{1}{\Psi_x - \Phi_x} + \frac{1}{\Psi_x - \Phi_y} \geq 0\,, \tag{18}$$

which leads to

$$q_x \cot q_x + q_y \cot q_y \geq 0\,, \tag{19}$$

which has been already determined in (Haghpanah et al., 2014). When the left hand side of (19) vanishes, the critical mode I, shown in Fig. 4, occurs.

This critical mode is not influenced neither by the axial stiffness of cables, since joint translations are null, or by their bending stiffness, which is negligible in view of (1).

ii) In this case we have $\beta_h = 0$ and $\omega_1 = 0$. The stability condition (15) reduces to

$$\left\{\beta_v^*, \theta^*\right\}\begin{bmatrix} k_{b22} + k & k_{b23} \\ k_{b23}^* & k_{b33} \end{bmatrix}\begin{Bmatrix} \beta_v \\ \theta \end{Bmatrix} \geq 0 \tag{20}$$

where k is the dimensionless stiffness of cables, given in Appendix B. The stability condition (20) is satisfied if and only if the following conditions

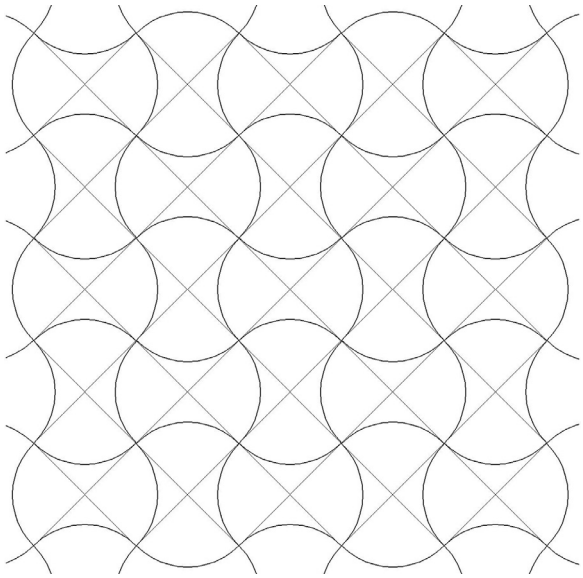

Fig. 4. Critical mode I.

holds:

$$k + k_{b22} = k + 4\frac{\left(1 - 8q_y^2(\Phi_y + \Psi_y)\right)}{\Phi_y + \Psi_y} \geq 0\,, \tag{21a}$$

$$\begin{aligned}
&(k_{b22} + k)k_{b33} - k_{b23}^* k_{b23} \\
&= 4\Bigg[\cos\omega_2 \frac{\left(k_c\Phi_v - 8q_y^2\Phi_v + 2\right)}{(\Phi_v - \Psi_v)(\Psi_v + \Phi_v)} \\
&- \frac{\left(\Psi_v\left(k_c - 8q_y^2\right)(\Psi_h + \Psi_v) + \Phi_h\left(k_c\Psi_v - 8q_y^2\Psi_v + 2\right)\right)}{(\Psi_h + \Phi_h)(\Phi_v - \Psi_v)(\Psi_v + \Phi_v)} \\
&+ \frac{\left(\Psi_v\left(-\Phi_v\left(k_c\Phi_v - 8q_y^2\Phi_v + 4\right) + 2(\Psi_h + 2\Psi_v)\right)\right)}{(\Psi_h + \Phi_h)(\Phi_v - \Psi_v)(\Psi_v + \Phi_v)}\Bigg] \geq 0\,.
\end{aligned} \tag{21b}$$

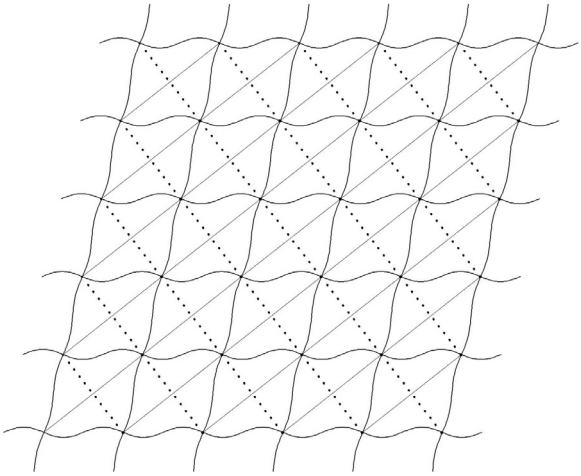

Fig. 5. Critical mode II.

Similarly to the previous case, the actual value of ω_2 must minimize the left hand side of (21b), which linearly depends on $\cos\omega_2$. For this reason the wave parameter ω_2 can only assume the values 0 or π. Then we get

$$k \geq k_v = \max(k_{v0}, k_{v\pi}, 0)\,, \tag{22}$$

where k_{v0} and $k_{v\pi}$ are the minimum values of k satisfying (21a) and (21b) in the two cases $\omega_2 = 0$ and $\omega_2 = \pi$ respectively. In particular

$$k_{v0} = 8q_y^3 \frac{q_x^2 \cot q_y + q_x q_y \cot q_x - q_y}{q_x q_y\left(q_x \cot q_y + q_y \cot q_x\right) - q_x^2 - q_y^2} \tag{23a}$$

$$k_{v\pi} = 8q_y^3 \frac{\cot q_y}{q_y \cot q_y - 1}\,. \tag{23b}$$

It can be shown that in any feasible state we always have $k_{v0} > k_{v\pi}$ and therefore ω_2 is always null. The critical mode associated to the condition $k = k_{v0}$ is represented in Fig. 5.

iii) Clearly, this case can be obtained from the previous case by a rigid rotation of $\pi/2$. Following a procedure similar to the previous case we find

$$k \geq k_h = \max(k_{h0}, k_{h\pi}, 0)\,, \tag{24}$$

where

$$k_{h0} = 8q_x^2 \frac{q_y^2 q_x \cot q_x + q_x q_y q_y \cot q_y - q_x}{q_x q_y\left(q_x \cot q_y + q_y \cot q_x\right) - q_x^2 - q_y^2} \tag{25a}$$

$$k_{h\pi} = 8q_x^2 \frac{q_x \cot q_x}{q_x \cot q_x - 1}\,. \tag{25b}$$

As in the previous case, in any feasible state here we find $\omega_1 = 0$ and $k_{h0} > k_{h\pi}$. The critical mode III, associated to the condition $k = k_{h0}$, can be obtained from the critical mode II by a rigid rotation of $\pi/2$.

5. Stability domain

From the preceding analysis we infer that the stability domain of this material is determined by the conditions

$$\begin{cases} q_x \cot q_x + q_y \cot q_y \geq 0 \\ k \geq \max(k_h, k_v) = \hat{k}(q_x, q_y) \end{cases}. \tag{26}$$

Now, the dimensionless macrostresses

$$\tilde{\Sigma}_x = \frac{\Sigma_x - \rho|T|}{\Sigma_E}, \quad \tilde{\Sigma}_y = \frac{\Sigma_y - \rho|T|}{\Sigma_E}\,, \tag{27}$$

are introduced, where

$$\Sigma_E = \frac{\pi^2 E}{12}\left(\frac{t}{l}\right)^3. \tag{28}$$

Then, in view of (14)

$$q_x = \frac{i\pi}{2}\sqrt{\tilde{\Sigma}_x}, \quad q_y = \frac{i\pi}{2}\sqrt{\tilde{\Sigma}_y}\,. \tag{29}$$

Since the dimensionless macrostresses $\tilde{\Sigma}_x$ and $\tilde{\Sigma}_y$ are always real quantities, whereas the parameters q_x and q_y are real positive or imaginary (if rods are compressed or tense, respectively), the stability domain defined by (26) must be represented in plane $(\tilde{\Sigma}_x, \tilde{\Sigma}_y)$ (see Fig. 6), where each point is associated to all macrostresses (Σ_x, Σ_y, T) satisfying (27).

Finally, it must be remarked that the stiffness k in (26) (see Appendix B) is sum of an elastic part $k_e > 0$ and a geometric part $k_T \geq 0$, proportional to the absolute value $|T|$ of the shear macrostress. To highlight this circumstance, in view of (14) and (57) the second of (26) is rewritten as

$$k_e\left[1 + \frac{\pi^2}{12 + k_e}\left(\frac{|T|}{\Sigma_E}\right)\right] \geq \bar{k}(\tilde{\Sigma}_x, \tilde{\Sigma}_x)\,. \tag{30}$$

where

$$\bar{k}(\tilde{\Sigma}_x, \tilde{\Sigma}_x) = \hat{k}\left(\frac{i\pi}{2}\sqrt{\tilde{\Sigma}_x}, \frac{i\pi}{2}\sqrt{\tilde{\Sigma}_y}\right).$$

Within the stability domain in Fig. 6 we can identify two zones: an inner zone where the minimum cable stiffness $\bar{k}(\tilde{\Sigma}_x, \tilde{\Sigma}_y)$ is null and an outer zone where $\bar{k}(\tilde{\Sigma}_x, \tilde{\Sigma}_y)$ is positive. Then in the inner zone the stability condition (30) is satisfied also for null values of k_e and the material is stable also in absence of cables. In this last case the modes II or III occur at the boundary of the inner zone (orange curve in Fig. 6), which is defined by the conditions

$$\begin{cases} k_{v0} = 0 \quad if \quad \tilde{\Sigma}_x \geq \tilde{\Sigma}_y \quad (mode\,II) \\ k_{h0} = 0 \quad if \quad \tilde{\Sigma}_x \leq \tilde{\Sigma}_y \quad (mode\,III) \end{cases} \tag{31}$$

which reduce to

$$\begin{cases} \dfrac{\cot q_x}{q_x} + \dfrac{\cot q_y}{q_y} - \dfrac{1}{q_x^2} = 0 \quad if \quad \tilde{\Sigma}_x \geq \tilde{\Sigma}_x \\ \dfrac{\cot q_x}{q_x} + \dfrac{\cot q_y}{q_y} - \dfrac{1}{q_y^2} = 0 \quad if \quad \tilde{\Sigma}_x \leq \tilde{\Sigma}_y \end{cases}, \tag{32}$$

already given in Haghpanah et al. (2014). In the outer zone of the domain cables are instead necessary for stability. We remark that, provided that the stability condition (30) holds, the boundary of the stability domain (blue curve in Fig. 6) is always determined by the occurrence of the critical mode I, which under the assumptions (1) is not influenced by the stiffness of cables.

In Figs. 7 and 8 the optimal dimensionless cable stiffness $\bar{k}(\tilde{\Sigma}_x, \tilde{\Sigma}_x)$, which is the minimum value ensuring stability, is represented. Fig. 8 clearly highlights the variation of $\bar{k}(\tilde{\Sigma}_x, \tilde{\Sigma}_x)$ on the boundary and in the outer zone of the stability domain. The minimum value of $\bar{k}$ on the boundary of the stability domain is attained at the point $A \equiv (-1, -1)$ and is equal to π^2, while the maximum value is attained at the limit points $(-4, \infty)$ and $(\infty, -4)$ and is $8\pi^2$. This value is also the maximum value of the optimal cable stiffness on the whole stability domain, so that if $k_e \geq 8\pi^2$ only the mode I can occur.

In Fig. 9, in the particular case $k_e = 8\pi^2$, we represent a portion the open frontier of stability domain of the material in the three dimensional space $\left(\frac{\Sigma_x}{\Sigma_E}, \frac{\Sigma_y}{\Sigma_E}, \frac{T}{\Sigma_E}\right)$. Clearly this frontier is always determined by the occurrence of the mode I.

6. Design and comparisons with FEM analysis

Now the critical states associated to the two points A and B (Figs. 6 and 7) are analyzed, with the aim of designing the metamaterial and of verifying the effectiveness of the simplifying assumptions which underly the proposed model. In particular, the obtained results has been verified by a finite element analysis (FEM) carried out by the software SAP2000, in which only a single cell has been considered. For each of the three critical modes occurring in this periodic metamaterial, specific kinematic conditions have been assigned to the boundary

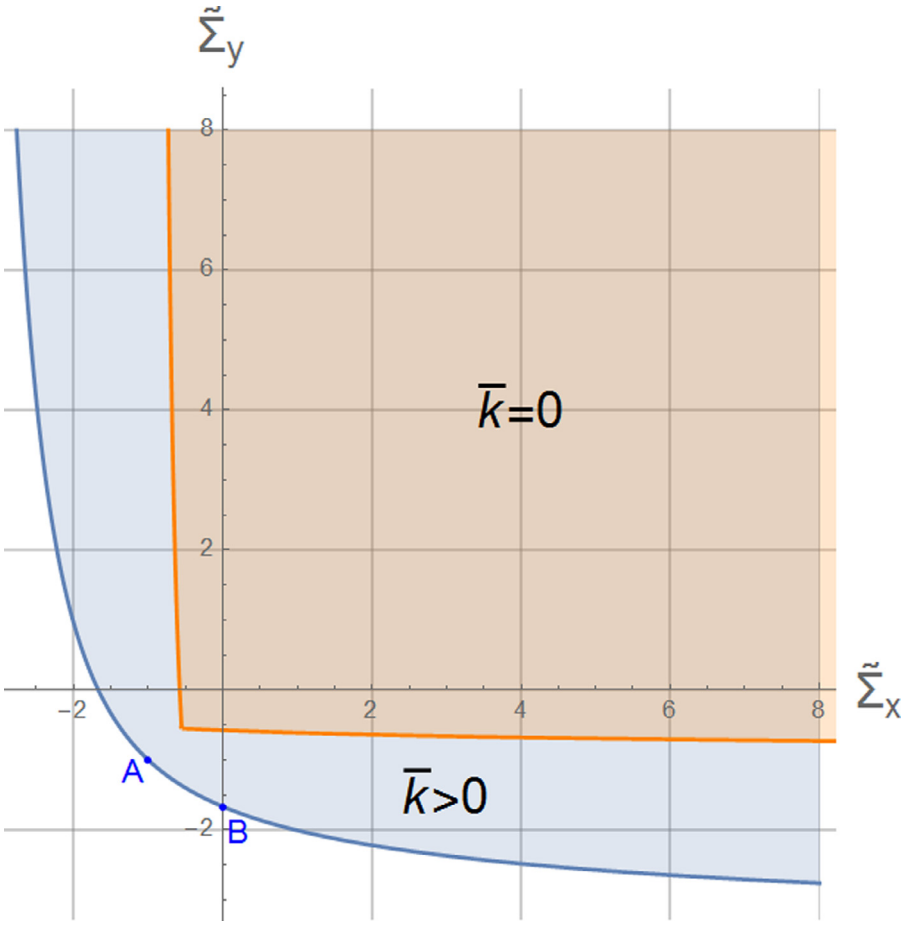

Fig. 6. Stability domain of the periodic material.

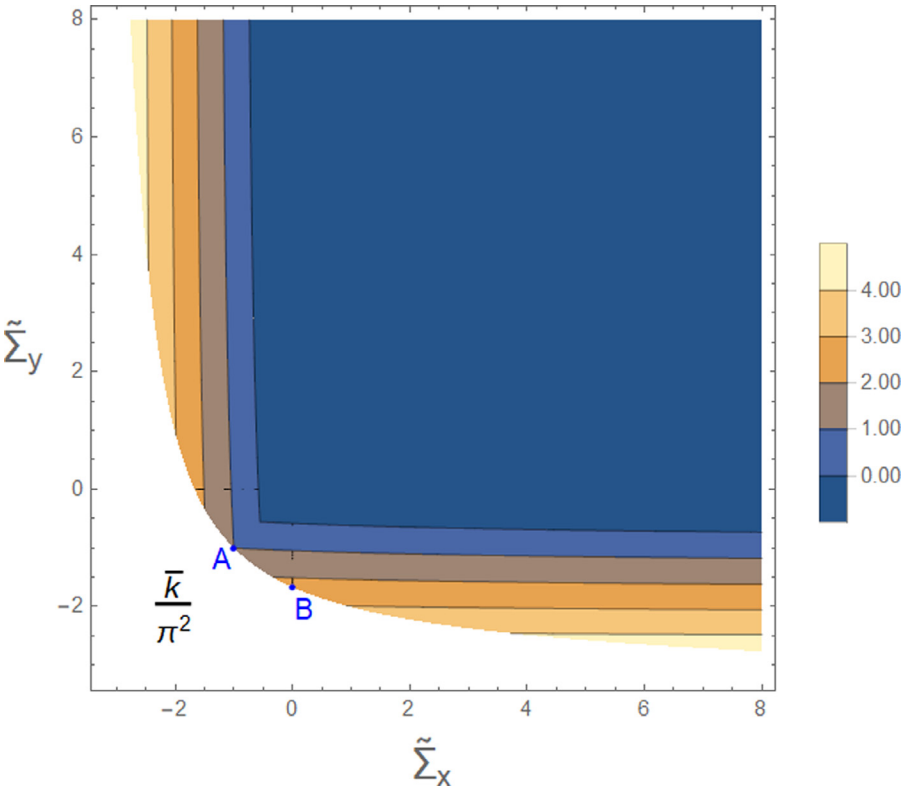

Fig. 7. Stability domain and optimal values $\bar{k}$.

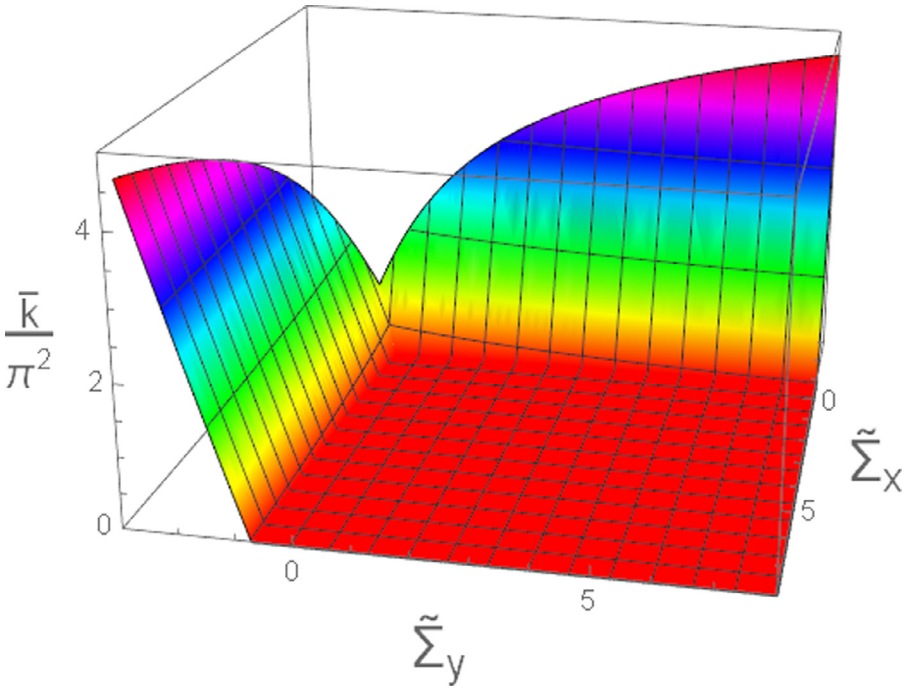

Fig. 8. Optimal values $\bar{k}$.

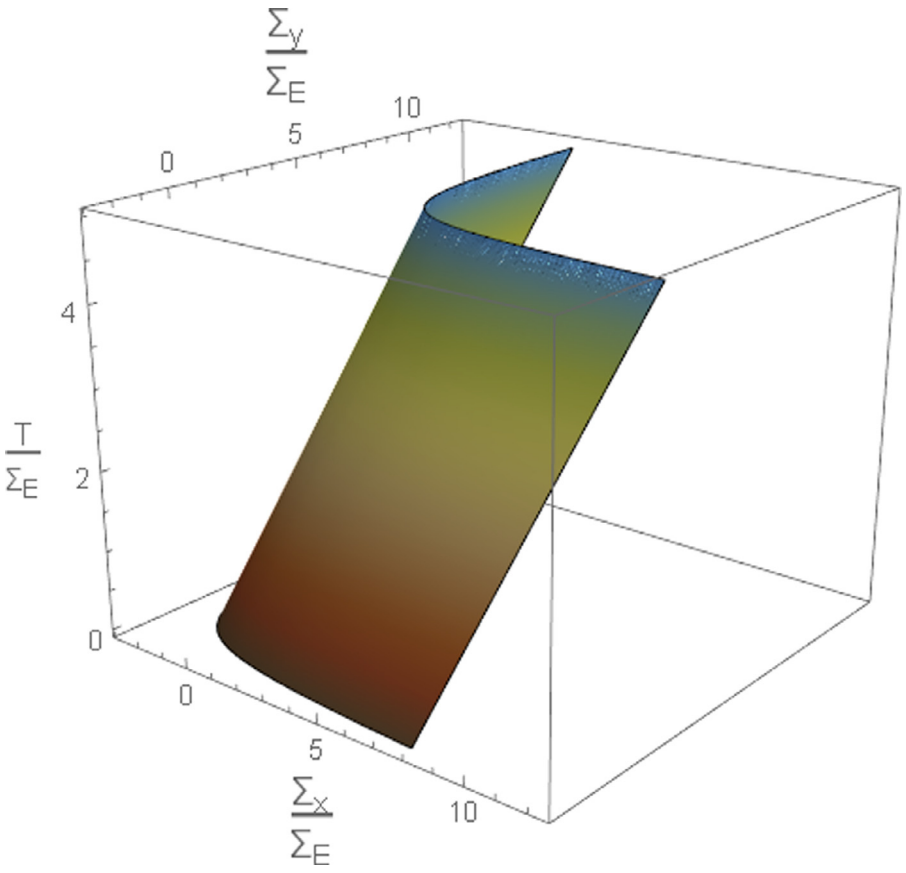

Fig. 9. Open frontier of the stability domain of the periodic material for $k_e = 8\pi^2$.

nodes of the cell (see Haghpanah et al., 2014), so assigning *a priori* the wavelength of the examined critical mode. A metamaterial with Young's modulus $E = 2800\ MPa$ and Poisson's ratio $\nu = 0.2$, in which rods have lengths $l = 10\ mm$ and thickness $t = 1\ mm$, has been selected. For it we find $\Sigma_E = 2.303\ MPa$.

The optimal design problem is not here addressed in a general setting, since it should be numerically solved and this is out of the scope of the present paper. However, for a given macrostress the minimum thickness of the cables $\bar{t}_c$ can be easily determined as the value yielding to the minimum elastic stiffness of cables $\bar{k}_e$ for which (30) is satisfied.

Therefore, from (54) in Appendix B we get

$$\frac{\bar{t}_c}{t} = \frac{\bar{k}_e}{6\sqrt{2}}\left(\frac{t}{l}\right)^2. \tag{33}$$

As already stated, at the point A the optimal value of the (dimensionless) cables stiffness is $\bar{k}(-1,-1) = \pi^2$. When the total stiffness of cables k attains the above optimal value π^2, the three modes I, II and III simultaneously occur in all macrostress states associated to this point, such that

$$-1 = \frac{\Sigma_x - \rho|T|}{\Sigma_E}, \quad -1 = \frac{\Sigma_y - \rho|T|}{\Sigma_E}. \tag{34}$$

Among all states satisfying (34) we consider only the equi-biaxial compression

$$(\Sigma_x = -\Sigma_E,\ \Sigma_y = -\Sigma_E,\ T = 0) \tag{35}$$

and the pure shear

$$\left(\Sigma_x = 0,\ \Sigma_y = 0,\ T = \frac{\Sigma_E}{\rho}\right). \tag{36}$$

In the equi-biaxial compression, (30) reduces to $\bar{k}_e = \pi^2$ and from (33) the minumum thickness ratio is $\bar{t}_c/t = 0.0116$.

In the pure shear state (36), the stability condition (30) reduces to $k_e + \pi^2 \geq \pi^2$, so the optimal value of the elastic stiffness of cables $\bar{k}_e$ vanishes and the minimum thickness of the cables $\bar{t}_c$ tends to zero. In this condition, in view of (5) also the distribution factor ρ vanishes and therefore the critical shear macrostress $T = \Sigma_E/\rho$ tends to infinity. Clearly, since cables and rods have finite strength, this design is not physically admissible. However, to verify the accuracy of the model we consider a suboptimal value of elastic cables stiffness fixed to $k_e = \frac{\pi^2}{100}$. So doing, in this critical state only the mode I occurs, while the modes I and II become nearly critical. FEM analysis has shown that in all examined cases the error between numerical and analytical results is about 1.5% and that it can be drastically reduced if shear deformations are annulled in FEM modeling.

The point B of coordinates $(0,-1.6681)$ is now examined. Here the optimal value of the total cables stiffness is $\bar{k}(0,-1.6681) = 2.3468\pi^2$. Considering this value, in all macrostress states such as

$$0 = \frac{\Sigma_x - \rho|T|}{\Sigma_E}, \quad -1.6681 = \frac{\Sigma_y - \rho|T|}{\Sigma_E}, \tag{37}$$

the two modes I and II simultaneously occur. Among the critical stress states satisfying (37) only the uniaxial compression

$$(\Sigma_x = 0,\ \Sigma_y = -1.6681\Sigma_E,\ T = 0) \tag{38}$$

and the biaxial state

$$\left(\Sigma_x = 0,\ \Sigma_y = \frac{-1.6681}{2}\Sigma_E,\ T = \frac{1.6681\Sigma_E}{2\rho}\right) \tag{39}$$

are here considered. In the uniaxial compression (38), stability condition (30) leads to $\bar{k}_e = 2.3468\pi^2$ and from (33) we find $\frac{\bar{t}_c}{t} = 0.0273$. In the biaxial state (39), the stability condition (30) reduces to

$$k_e\left[1 + \frac{1.6681\pi^2}{2k_e}\right] \geq 2.3468\pi^2, \tag{40}$$

which leads to the optimal value of the elastic stiffness $\bar{k}_e = 1.51275\pi^2$ and subsequently to the minimal thickness ratio $\bar{t}_c/t = 0.0176$.

Also in these last two cases the error between the FEM results and analytic results is about 1.5% and it is essentially due to the absence of shear deformability in our modeling.

Conclusions

In this paper a metamaterial obtained by coupling a periodic square mesh of rods with a periodic pattern of diagonal cables has been studied. By introducing some simplifying assumptions, whose effectiveness has been confirmed by FEM analysis, closed form solutions for the critical modes and the stability domain have been determined. The obtained solutions have allowed us to address the optimal design of this metamaterial, whose stability performance has been significantly improved by the coupling with cables.

Declaration of Competing Interest

The authors declare that they have no known competing financial interests or personal relationships that could have appeared to influence the work reported in this paper.

Acknowledgment

This investigation has been supported by the Research Project of National Relevance “Multiscale Innovative Materials and Structures” granted by the Italian Ministry of Education, University and Research (MIUR Prin 2017, project code 2017J4EAYB).

Appendix A. Rod stiffness matrix of a unit cell

Let us consider a generic inextensible beam of length l, subjected to an axial compressive load P and to the bending moments M_a and M_b at the end sections, as shown in Fig. 10. Since rigid translations are inessential, the *rigid* rotation β and the rotations of the end sections ϑ_a and ϑ_b can be assumed as degrees of freedom.

The following relations (see Stephen P. Timoshenko, 2009) can be established

$$\begin{cases} \vartheta_a - \beta = m_a\Psi(q) + m_b\Phi(q) \\ \vartheta_b - \beta = m_a\Phi(q) + m_b\Psi(q) \\ \beta = -\frac{m_a+m_b+s}{4q^2} \end{cases} \tag{41}$$

where:

$$\begin{aligned} &\Phi(q) = \frac{1}{2q}\left(\frac{1}{2q} - \frac{1}{\sin 2q}\right),\ \Psi(q) = \frac{1}{2q}\left(\frac{1}{2q} - \frac{1}{\tan 2q}\right), \\ &m_a = \frac{M_a l}{EJ},\ m_b = \frac{M_b l}{EJ},\ s = \frac{Sl^2}{EJ}, \\ &q = \frac{l}{2}\sqrt{\frac{P}{EJ}} \end{aligned} \tag{42}$$

From (41), we get

$$\begin{Bmatrix} m_a \\ m_b \\ s \end{Bmatrix} = \begin{bmatrix} \frac{\Psi(q)}{\Psi(q)^2-\Phi(q)^2} & \frac{\Phi(q)}{\Phi(q)^2-\Psi(q)^2} & -\frac{1}{\Phi(q)+\Psi(q)} \\ \frac{\Phi(q)}{\Phi(q)^2-\Psi(q)^2} & \frac{\Psi(q)}{\Psi(q)^2-\Phi(q)^2} & -\frac{1}{\Phi(q)+\Psi(q)} \\ -\frac{1}{\Phi(q)+\Psi(q)} & -\frac{1}{\Phi(q)+\Psi(q)} & \frac{2}{\Phi(q)+\Psi(q)} - 4q^2 \end{bmatrix} \begin{Bmatrix} \vartheta_a \\ \vartheta_b \\ \beta \end{Bmatrix}, \tag{43}$$

that can be also written as

$$\left(\frac{l}{EJ}\right)\begin{Bmatrix} M_a \\ M_b \\ Sl \end{Bmatrix} = \hat{\boldsymbol{k}}(q)\begin{Bmatrix} \vartheta_a \\ \vartheta_b \\ \beta \end{Bmatrix} = \hat{\boldsymbol{k}}(q)\boldsymbol{\delta}. \tag{44}$$

Now, from (7) the kinematic relations $\boldsymbol{\gamma} = \boldsymbol{T}_j\boldsymbol{\delta}_j$ between the cell degrees of freedom vector $\boldsymbol{\gamma}$ and the rods degrees of freedom vectors $\boldsymbol{\delta}_{j\ (j=1,2,3,4)}$ can be established (see Fig. 11), where the matrices $\boldsymbol{T}_j$ have the following expressions

$$\begin{aligned} &T_1 = \begin{bmatrix} 0 & 0 & e^{i\omega_1} \\ 0 & 0 & 1 \\ 1 & 0 & 0 \end{bmatrix},\ T_2 = \begin{bmatrix} 0 & 0 & 1 \\ 0 & 0 & e^{-i\omega_1} \\ e^{-i\omega_1} & 0 & 0 \end{bmatrix}, \\ &T_3 = \begin{bmatrix} 0 & 0 & e^{i\omega_2} \\ 0 & 0 & 1 \\ 1 & 0 & 0 \end{bmatrix},\ T_4 = \begin{bmatrix} 0 & 0 & 1 \\ 0 & 0 & e^{-i\omega_2} \\ e^{-i\omega_2} & 0 & 0 \end{bmatrix}. \end{aligned} \tag{45}$$

The rods stiffness matrix of the cell is then determined as

$$\boldsymbol{k}_b = \sum_{j=1}^{4} \boldsymbol{T}_j^H\,\hat{\boldsymbol{k}}_j\boldsymbol{T}_j, \tag{46}$$

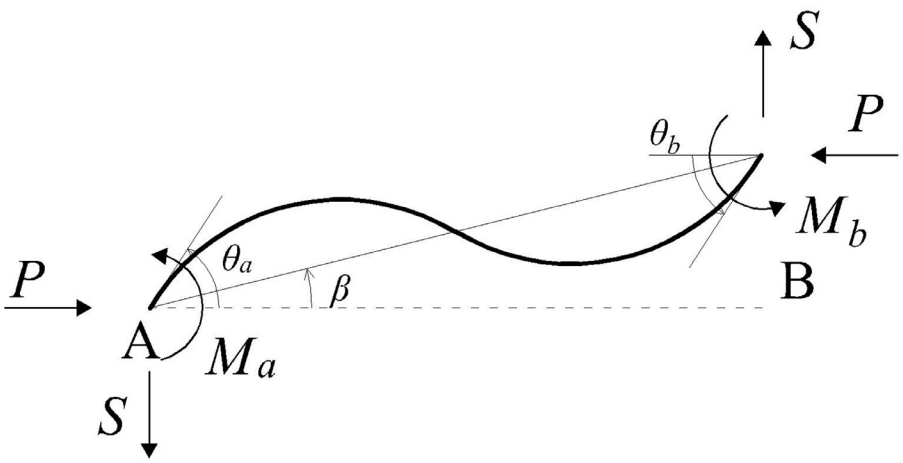

Fig. 10. Free inexentsible beam.

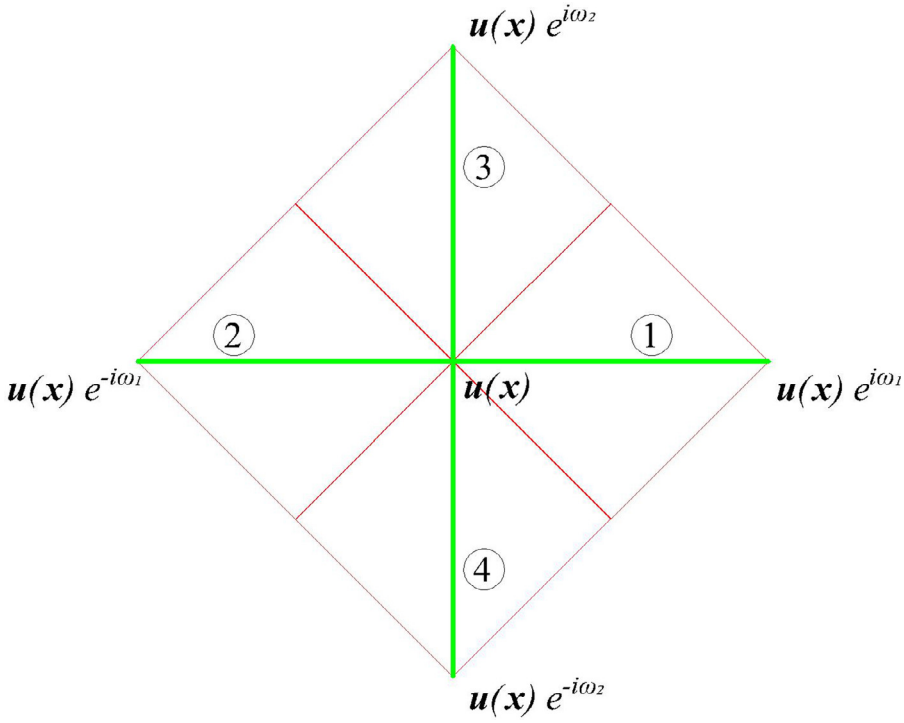

Fig. 11. Displacements of the joints of type *1* in a periodic cell and numeration of the rods.

where

$$\hat{\boldsymbol{k}}_1 = \hat{\boldsymbol{k}}_2 = \hat{\boldsymbol{k}}(q_x), \quad \hat{\boldsymbol{k}}_2 = \hat{\boldsymbol{k}}_3 = \hat{\boldsymbol{k}}(q_y), \tag{47}$$

q_x and q_y are given in (14) and $\boldsymbol{T}_a^H$ are the conjugate transposes of $\boldsymbol{T}_a$. From (45), (46) and (47) we find the hermitian matrix

$$\boldsymbol{k}_b = \begin{bmatrix} k_{b11} & 0 & k_{b13} \\ 0 & k_{b22} & k_{b23} \\ k_{b13}^* & k_{b23}^* & k_{b33} \end{bmatrix},$$

$$k_{b11} = \frac{4(1 - 8q_x^2(\Phi_x + \Psi_x))}{\Phi_x + \Psi_x}, \qquad k_{b13} = -\frac{2(\cos\omega_1 + i\sin\omega_1 + 1)}{\Phi_x + \Psi_x},$$

$$k_{b22} = \frac{4\left(1 - 8{q_y}^2(\Phi_y + \Psi_y)\right)}{\Phi_y + \Psi_y}, \qquad k_{b23} = -\frac{2(\cos\omega_2 + i\sin\omega_2 + 1)}{\Phi_x + \Psi_x},$$

$$k_{b33} = 4\left(\frac{\Psi_x - \Phi_x\cos\omega_1}{\Psi_x^2 - \Phi_x^2} + \frac{\Psi_y - \Phi_y\cos\omega_2}{\Psi_y^2 - \Phi_y^2}\right), \tag{48}$$

where

$$\begin{aligned} \Psi_x &= \Psi(q_x), \qquad \Phi_x = \Phi(q_x) \\ \Psi_y &= \Psi(q_y), \qquad \Phi_y = \Phi(q_y) \end{aligned}. \tag{49}$$

Appendix B. Stiffness of cables

The dimensionless cables stiffness matrix $\boldsymbol{k}_c$ is here determined. Let us recall that in view of (1) only traction forces can be exerted by cables and the bending stiffness of cables is negligible with respect that of the rods. For sake of semplicity, let us consider the scheme in Fig. 12 in which we set $\beta_h = 0$. The cables with indexes from 5 to 8 are in traction (continuous thin lines), while the other cables (dotted lines) are buckled.

The virtual work of the cable traction forces can be written as

$$K\,\beta_v^*\beta_v, \tag{50}$$

where K is the total stiffness of the cables in a cell. Now let us introduce the dimensionless stiffness of cables k

$$k = \left(\frac{l}{EJ}\right)K, \tag{51}$$

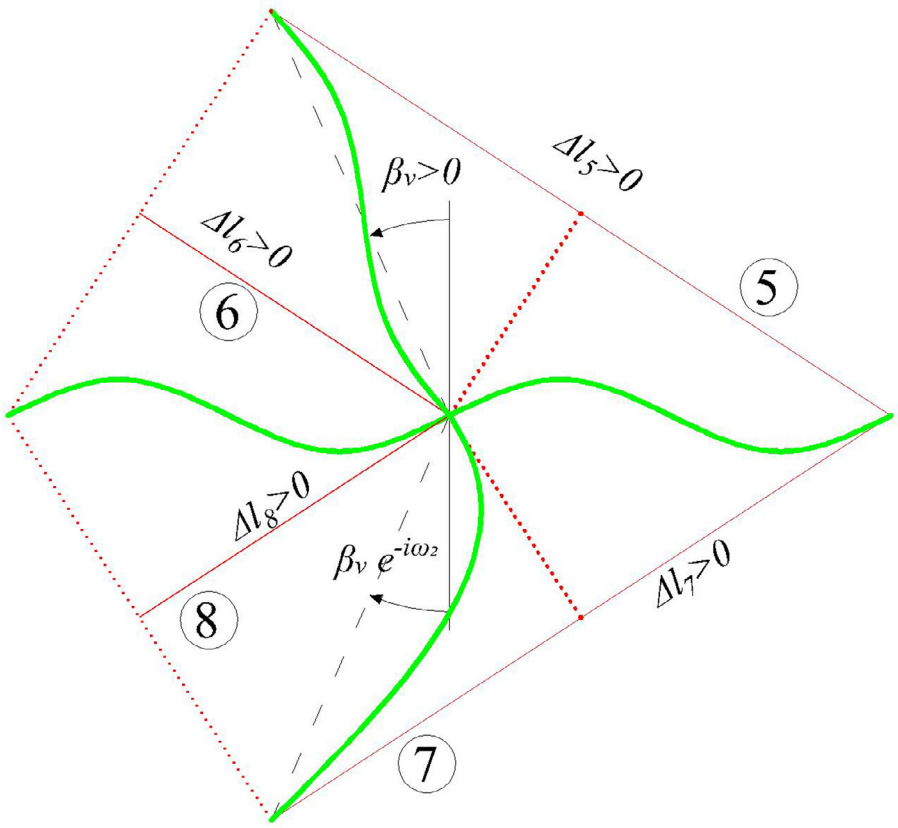

Fig. 12. Cables in tractions and cables buckled in a cell.

which is sum of an elastic term k_e and a geometric term k_T depending on the traction forces N_T, given in (4):

$$k = k_e + k_T\,. \tag{52}$$

Since the stiffnesses and the axial forces of the cables 5 and 7 are halved, we find

$$\begin{aligned}\beta_v^* k \beta_v = \left(\frac{l}{EJ}\right) \quad & \left[\frac{l\beta_v^*}{\sqrt{2}}\left(\frac{EA_c+N_T}{2\sqrt{2}l}\right)(1+e^{-i\omega_2}e^{i\omega_2})\frac{l\beta_v}{\sqrt{2}}\right.\\ & \left.+\frac{l\beta_v^*}{2\sqrt{2}}\left(\frac{EA_c+N_T}{l/\sqrt{2}}\right)(1+e^{-i\omega_2}e^{i\omega_2})\frac{l\beta_v}{2\sqrt{2}}\right]\\ & = \left(\frac{l}{EJ}\right)\frac{(EA_c+N_T)l}{\sqrt{2}}\beta_v^*\,\beta_v \quad .\end{aligned} \tag{53}$$

From which we get the dimensionless elastic stiffness

$$k_e = \frac{EA_c l^2}{EJ\sqrt{2}} = 6\sqrt{2}\left(\frac{t_c}{t}\right)\left(\frac{l}{t}\right)^2 \tag{54}$$

and the dimensionless geometric stiffness that, in view of (4), becomes

$$k_T = \frac{N_T l^2}{EJ\sqrt{2}} = \left(\frac{\pi^2\rho}{\Sigma_E}\right)|T|\,. \tag{55}$$

By analyzing the general case in which both β_h and β_v are not null, the cable stiffness matrix is determined as

$$\boldsymbol{k}_c = \begin{bmatrix} k & -k & 0\\ -k & k & 0\\ 0 & 0 & 0\end{bmatrix}, \tag{56}$$

where, from (4), (54) and (55)

$$k = k_e\left[1+\frac{\pi^2}{12+k_e}\left(\frac{|T|}{\Sigma_E}\right)\right] \tag{57}$$

Appendix C. Distribution factor ρ

As usual in Eulerian stability analysis, in precritical states the mechanical response of the metamaterial is assumed linear. Then the distribution factor ρ is determined with reference to the unstressed initial state in which the stiffness of cables reduces to its elastic part k_e only, which is given in (54). In this state wave length is infinite in both directions ($\boldsymbol{\omega}=\mathbf{0}$) and, since rigid rotations are inessential, we assume $\beta_h = 0$. Then in a precritical shear macrostress the joint displacements can be determined as

$$\begin{Bmatrix}\beta_v\\ \theta\end{Bmatrix} = \left(\frac{l}{EJ}\right)\boldsymbol{k}_{II}^{-1}(\mathbf{0},0,0)\begin{Bmatrix}2Tl^2\\ 0\end{Bmatrix}, \tag{58}$$

where $\boldsymbol{k}_{II}$ is formed by the last two rods and the last two columns of $\boldsymbol{k}$. From (58) we find

$$\begin{Bmatrix}\beta_v\\ \theta\end{Bmatrix} = \frac{2Tl^2}{12+k_e}\begin{Bmatrix}1\\ 1/2\end{Bmatrix} \tag{59}$$

and then

$$N_T = \frac{EA_c}{\sqrt{2}l}\frac{l|\beta_v|}{\sqrt{2}} = \sqrt{2}\frac{k_e}{12+k_e}|T|l \tag{60}$$

which leads to (5).

References

Amendola, A., Krushynska, A., Daraio, C., Pugno, N., Fraternali, F., 2018. Tuning frequency band gaps of tensegrity metamaterials with local and global prestress. 1803.03472v1([nlin.PS]).

Bordiga, G., Cabras, L., Piccolroaz, A., Bigoni, D., 2020. Incremental constitutive tensors and strain localization for prestressed elastic lattices: part ii – incremental dynamics. 2001.02151.

Boukadia, R.F., Deckers, E., Claeys, C., Ichchou, M., Desmet, W., 2020. A wave-based optimization framework for 1d and 2d periodic structures. Mech. Syst. Signal Process. 139.

Chen, H., Chan, C., Sheng, P., 2010. Transformation optics and metamaterials. Nat. Mater. 9, 387–396.

Cummer, S., Christensen, J., Alú, A., 2016. Controlling sound with acoustic metamaterials. Nat. Rev. Mater. 1.
DeTommasi, D., Marano, G., Puglisi, G., Trentadue, F., 2017. Morphological optimization of tensegrity-type metamaterials. Compos. Part B: Eng. 115, 182–187.
DeTommasi, D., Puglisi, G., Trentadue, F., 2018. Elastic moduli of optimal tensegrity-type metamaterials. Front. Mater. submitted, 1041–1048.
Fang, N., Xi, D., Xu, J., Ambati, M., Srituravanich, W., Sun, C., Zhang, X., 2006. Ultrasonic metamaterials with negative modulus. Nat. Mater. 5, 452–456.
Fraternali, F., Carpentieri, G., Amendola, A., Skelton, R., Nesterenko, V., 2014. Multiscale tunability of solitary wave dynamics in tensegrity metamaterials. Appl. Phys. Lett. 105, 201903.
Fraternali, F., Senatore, L., Daraio, C., 2012. Solitary waves on tensegrity lattices. J. Mech. Phys. Solids 60, 1137–1144.
Geymonat, G., Mller, S., Triantafyllidis, N., 1993. Homogenization of nonlinearly elastic materials, microscopic bifurcation and macroscopic loss of rank-one convexity. Arch. Ration. Mech. Anal. 122 (3), 231–290.
Gong, L., Kyriakides, S., Triantafyllidis, N., 2005. On the stability of kelvin cell foams under compressive loads. J. Mech. Phys. Solids 53 (4), 771–794.
Haghpanah, B., Papadopoulos, J., Mousanezhad, D., Nayeb-Hashemi, H., Vaziri, A., 2014. Buckling of regular, chiral and hierarchical honeycombs under a general macroscopic stress state. Proc. R. Soc. A: Math. Phys. Eng. Sci. 470 (2167), 20130856.
Hutchinson, R.G., Fleck, N.A., 2006. The structural performance of the periodic truss. J. Mech. Phys. Solids 54 (4), 756–782.
Krushynska, A., Bosia, F., Miniaci, M., Pugno, N., 2017. Spider web-structured labyrinthine acoustic metamaterials for low-frequency sound control. New J. Phys. 19 (105001).
Liu, J., Bertoldi, K., 2015. Bloch wave approach for the analysis of sequential bifurcations in bilayer structures. Proc. R. Soc. A: Math. Phys. Eng. Sci. 471 (2182).
Paulose, J., Meeussen, A., Vitelli, V., 2015. Selective buckling via states of self-stress in topological metamaterials. PNAS 112, 7639–7644.
Schittny, R., Buckmann, T., Kadic, M., Wegener, M., 2013. Elastic measurements on macroscopic three-dimensional pentamode metamaterials. Appl. Phys. Lett. 30 (103), 11905.
Stephen P. Timoshenko, J.M.G., 2009. Theory of Elastic Stability, 2 Dover Publications.
Triantafyllidis, N., Schraad, M.W., 1998. Onset of failure in aluminum honeycombs under general in-plane loading. J. Mech. Phys. Solids 46 (6), 1089–1124.
Wang, A.-J., McDowell, D., 2004. In-plane stiffness and yield strength of periodic metal honeycombs. J. Eng. Mater. Technol. 126 (2), 137–156.